Translational Oncology 27 (2023) 101570

Contents lists available at ScienceDirect

Translational Oncology

journal homepage: www.elsevier.com/locate/tranon

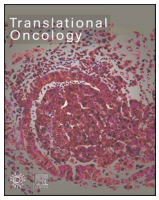

Original Research

Multiregion single cell analysis reveals a novel subtype of cancer-associated fibroblasts located in the hypoxic tumor microenvironment in colorectal cancer

Nanxin Zheng [a,1], Rongbo Wen [a,1], Leqi Zhou [a,1], Qingying Meng [a], Kuo Zheng [a], Zhixuan Li [b], Fuao Cao [a], Wei Zhang [a,*]

[a] Department of Colorectal Surgery, Changhai Hospital, Naval Medical University, Shanghai, China
[b] Translational Medicine Research Center, Medical Innovation Research Division and Fourth Medical Center of the Chinese PLA General Hospital, Beijing, China

ARTICLE INFO

Keywords:
Colorectal cancer
Tumor microenvironment
Cancer-associated fibroblasts
Hypoxia

ABSTRACT

Background: : The tumor microenvironment (TME) plays a critical role in shaping tumor progression and determining the outcome of the therapeutic response. In this study, we aimed to generate a comprehensive cellular landscape of the colorectal cancer (CRC) TME.

Methods: : We generated a comprehensive single-cell atlas by collecting CRC cases that have been uploaded to the online database and conducting an in-depth secondary analysis. We then carried out spatial transcriptomic sequencing and multiple immunohistochemical analyses to verify the results of the single-cell analysis. Moreover, we applied our findings to the TCGA database and used tissue microarray (TMA) on CRC tissue specimens to validate clinical prognosis.

Findings: We re-analyzed the transcriptomes of 23785 cells, revealing a pattern of cell heterogeneity in the tumor region, leading-edge region, and non-tumor region. A subtype of *COL11A1*+*INHBA*+ tumor-resident cancer-associated fibroblasts (CAFs) was identified, and marker genes, transcription factors, and tissue-specific expression differences were noted and suggested to have potential roles in promoting cancer. We further confirmed that *COL11A1*+*INHBA*+ tumor-resident CAFs are mainly located in the hypoxic TME and we propose that they interact with *CD44*+ CRC cells via INHBA. Elevation of INHBA in CRC is associated with a poor prognosis.

Interpretation: : Our results demonstrated a single cell landscape of CRC in different regions and identified in hypoxic TME a special subtype of CAFs producing INHBA, which promotes CRC development and correlates with poor prognosis. This special subtype of CAFs is a candidate target for translational research.

Introduction

Colorectal cancer (CRC) is the third most common cancer worldwide and the leading cause of global cancer morbidity and mortality [1]. Despite continuous improvements in surgery, chemotherapy, radiotherapy, and targeted therapy, a significant proportion of CRC patients develop drug resistance and their disease relapses over the course of treatment [2], which emphasizes the need for a better understanding of the mechanisms underlying CRC metastasis.

Over the past years, it has been proposed that the tumor microenvironment (TME) plays a pivotal role in CRC drug resistance and relapse [3]. The complex communication between the TME and cancer cells has far-reaching consequences for the progression and spread of CRC [4]. During the early stages of tumorigenesis, a finely tuned repertoire of cytokines and their receptors maintain the homeostatic balance between the TME and cancer cells [5]. This balance can be destroyed by selective pressures, leading to activation of carcinoma-associated fibroblasts (CAFs), which are the dominant component of the TME. CAFs secrete

Abbreviation: CAF, carcinoma-associated fibroblasts; CRC, colorectal cancer; CSCs, cancer stem cells; MFs, myofibroblasts; migDCs, migratory dendritic cells; scRNA-seq, single-cell RNA sequence analysis; TME, tumor microenvironment.

* Corresponding author.
E-mail address: weizhang2000cn@163.com (W. Zhang).

[1] These authors contributed equally to this work.

https://doi.org/10.1016/j.tranon.2022.101570
Received 18 June 2022; Received in revised form 8 October 2022; Accepted 12 October 2022

various stromal factors, contributing to the maintenance of colorectal cancer stem cells (CSCs), chemoresistance, and promoting metastasis [6]. Targeting bidirectional crosstalk may be a useful strategy for CRC therapy. However, CAFs in CRC are inhomogeneous and have different phenotypes and functions [7], and there is a lack of markers that accurately reflect their biological sources and functions [3,8,9]. Understanding the features that differentiate CAFs and the mechanisms by which CAFs regulate colorectal CSCs currently limits the pioneering efforts to develop drugs targeting CAFs.

Here, we performed a comprehensive single-cell analysis of publicly available data on CRC samples and identified a cancer-promoting heterogeneous cluster of CAFs. *COL11A1* and *INHBA* are specifically expressed in these heterogeneous cluster CAFs, and elevation of these markers in CRC is associated with a poor prognosis. Heterogeneous clusters of CAFs are located in the hypoxic TME and may interact with *CD44*+ CRC cells. The interaction of INHBA secreted by heterogeneous clusters of CAFs and ACVR on *CD44*+ CRC cells might play an important role in maintaining colorectal CSCs, and thereby promote colorectal tumor development.

Results

Single-cell landscape of colorectal carcinoma in different regions

The colorectal carcinoma (CRC) microenvironment is a complex niche composed of parenchymal and mesenchymal cells, and in which the cellular composition remains highly heterogeneous. A comprehensive analysis of the distribution and subtypes of cells across disparate regions can help us to better understand the ontogeny and development of CRC and more efficiently identify therapeutic targets. For this reason, we used seven CRC scRNA-seq datasets that were uploaded to the online database to conduct an in-depth secondary analysis. The three CRC tissue sites in each case were T (tumor) region, L (leading-edge) region, and N (non-tumor) region. Overall, 23785 cells that passed the quality control inspection were eligible for subsequent analysis, yielding 22875 detectable genes. Spatial transcriptomic sequencing was also performed to verify our findings.

To better probe the quantitative changes of different cell clusters within CRC, unified manifold approximation and projection (UMAP) dimensionality reduction was implemented in the "Seurat" package to visualize clustering of cells among different regions from all samples (**Fig. 1a**). The percentage of cell types in each sample is shown in **Fig. 1d**. All major cell types can be compared between different regions and samples, albeit at different proportions. Based on the expression of canonical genes, these clusters were annotated into eight main cell types: T/NK cells (*CD3D, NKG7*, and *KLRD1*), B/plasma cells (*JCHAIN, MS4A1*, and *CD79A*), myeloid cells (*LYZ*), epithelial cells (*EPCAM*), myofibroblasts (*DCN* and *COL1A1*), endothelial cells (*VWF*), enteric glial cells (*S100B*), and stem-like cells (*KIT*) (**Fig. 1a, b**). The representative top 5 genes are shown in **Fig. 1c**. To further explore the heterogeneity of cells in different niches of CRC, a scatter plot of the differences in the proportion of cells across different sites was drawn for each cluster (**Fig. 1e**). Interestingly, compared with the L and N regions, we observed that the proportion of plasma cells (C01) decreased dramatically in the T region. As for myofibroblast cells, C12 was enriched in the T and L regions, whereas C07 was substantially reduced, suggesting that tumor-associated fibroblasts (CAFs) and normal myofibroblasts (MFs) were replaced in different regions. In the T and L regions, T cells from C09 with high expression of *TNFRSF4, TNFRSF18, BATF* and *IL13* were predominantly enriched. Additionally, enteric glial cells were absent in the tumor. Although the number remained low, the proportion of migratory dendritic cells (migDCs) expressing *FSCN1* was significantly higher in the L region.

Identification of CRC parenchymal cells and hypoxia-induced JAK-STAT pathway activation in CD44+ stem cells

We sorted cells with an epithelial phenotype based on the expression level of *EPCAM* (**Fig. 2a**), and inferred copy number variation for each cell using the 'inferCNV' package. As shown in **Fig. 2a**, clusters of malignant cells were only from CRC01, CRC02, CRC03, and CRC04, just because no cancer cells were found in the original sequencing data of CRC05, CRC06, and CRC07. Correspondingly, cells were categorized as non-malignant (E06, E08, and E10) and malignant cells (C01, C02, C03, C04, C05, C07, and C09) (**Fig. 2b**), which was further determined by the distributional differences across regions (**Fig. 2c**). We found that non-malignant cells from different samples were discretely distributed among different dimensionality reduction clusters, whereas normal tissues adjacent to cancer were located in the same clusters. Compared to non-malignant cells, CRC malignant cells showed evident heterogeneity among individuals. Although there was no dense distribution of malignant cells, epithelial tissues adjacent to cancer cells had sporadic alterations in copy number, whereas there was no clonal proliferation or heterogeneity in the transcriptome (**Fig. 2b**).

Next, we calculated the cell cycle score (G1, G2M, and S) and differentiation (epithelial or mesenchymal) score for each cell and assigned each cell to a specific cycle and differentiation stage (**Fig. 2d and e**). When compared with para-cancer tissues, the inter-individual heterogeneity of tumors is also reflected in the divergence of the proliferation and differentiation states. It should be noted that the cell cycle or differentiation stage of cells in T and L regions in the same individual is not the same, and there is no identical underlying rule generalizable to all samples, which may be attributed to intra-tumor heterogeneity. Therefore, we explored intratumoral heterogeneity among these seven samples, from which sufficient malignant cells were collected from CRC01, CRC02, CRC03, and CRC04. Except for CRC04, which had only one cluster, the other three samples could be divided into two or three clusters in which differences in the transcriptome were observed. Among the three clusters of CRC01, C07 cells highly expressed *CTSE, PI3, SLPI*, and *IFI6*, whereas C11 cells highly expressed *LMO7, N4BP2L2, HSPA5*, and *NEAT1*. When the two clusters from CRC02 were compared, C05 cells were characterized by high expression levels of *RP11-462G2.1, UBE2C, CBX3*, and *CKS2*. In the two CRC03 clusters, C09 cells expressed high levels of *IGFBP3, PSCA, KRT16*, and *NEAT1* (**Fig. 2f**). Intriguingly, both C09 and C11 cells had upregulated expression of *NEAT1*, in agreement with our previous studies in liver cancer organoid models [10], and the elevated expression of *NEAT1* was mainly co-expressed with *CD44*+ stem cells (**Fig. 2g**). Elevated expression of *NEAT1* is associated with hypoxia [10]. Consistent with these findings, the upregulated genes of C09 and C11 were subjected to KEGG pathway enrichment, with the results indicating hypoxia-induced activation of the HIF1 signaling pathway (**Fig. 2h**). It was reported in our previous studies that upregulation of *NEAT1* could also activate the JAK-STAT pathway downstream, thereby facilitating drug resistance and proliferation in stem cells [10]. We further found an enriched expression of genes related to the JAK-STAT signaling pathway in the C09 and C11 clusters, suggesting that the hypoxic environment might be related to stemness remodeling in primary CRC (**Fig. 2i**).

Negative immune regulation and lack of antigen presentation

Alterations in the immune microenvironment of CRC are critical in the ontogeny and development of malignancy. Notably, many studies have reported immunosuppressive states and a lack of antigen presentation in the core of tumors. This study specifically addressed changes in the cellular composition of immune cells in CRC, which is rarely observed in a stepwise manner. Thus, we identified and mapped clusters and the composition of T/natural killer (NK) cells, B/plasma cells, and myeloid cells in the T, L, and N regions of CRC (**Fig. 3a**).

We categorized T/NK cells into 15 clusters (T01-T15), including

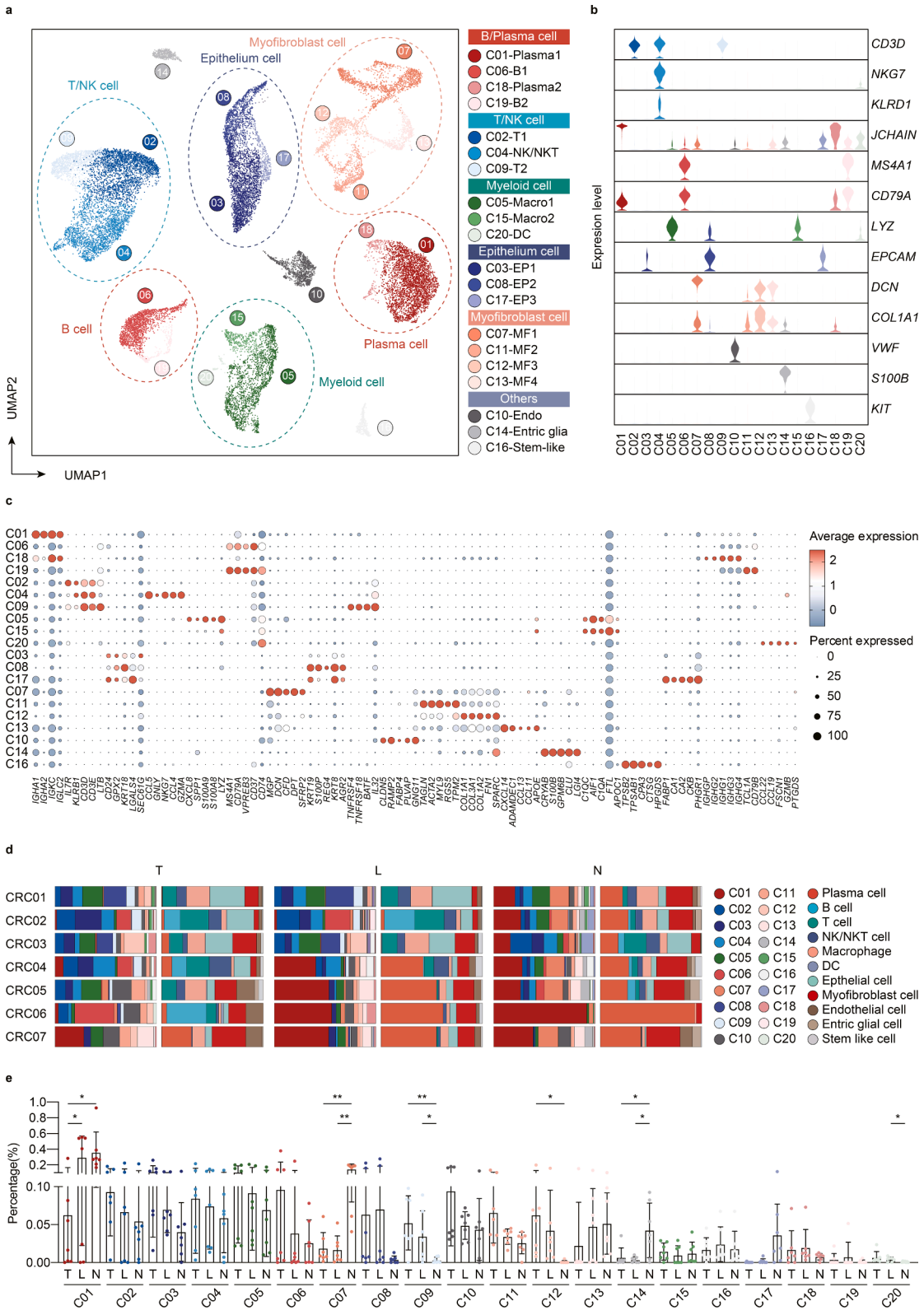

Fig.1. Single cell landscape of colorectal carcinoma (CRC) in different regions.

a. Distribution of 20 cell clusters on UMAP plot including B/plasma cells (C01, C06, C18, C19), T/NK cells (C02, C04, C09), Myeloid cells (C05, C15, C20), Epithelium cells (C03, C08, C17), Myofibroblast cells (C07, C11, C12, C13), Endothelial cells (C10), Enteric glial cells (C14) and Stem-like cells (C16).

b. Violin plots displaying marker genes (B/plasma cells: *JCHAIN, MS4A1, CD79A*, T/NK cells: *CD3D, NKG7, KLRD1*, Myeloid cells: *LYZ*, Epithelium cells: *EPCAM*, Myofibroblast cells: *DCN, COL1A1*, Endothelial cells: *VWF*, Enteric glial cells: *S100B*, Stem-like cells: *KIT*).

c. Dot plot of top5 genes in each cluster.

Distribution and composition of clusters and different cell types in T (Tumor region), L (Leading-edge region) and N (Non-tumor region) among 7 samples.

d. Scatter plot and statistical differences of 20 clusters ($p < 0.05$: * and $p < 0.01$: **).

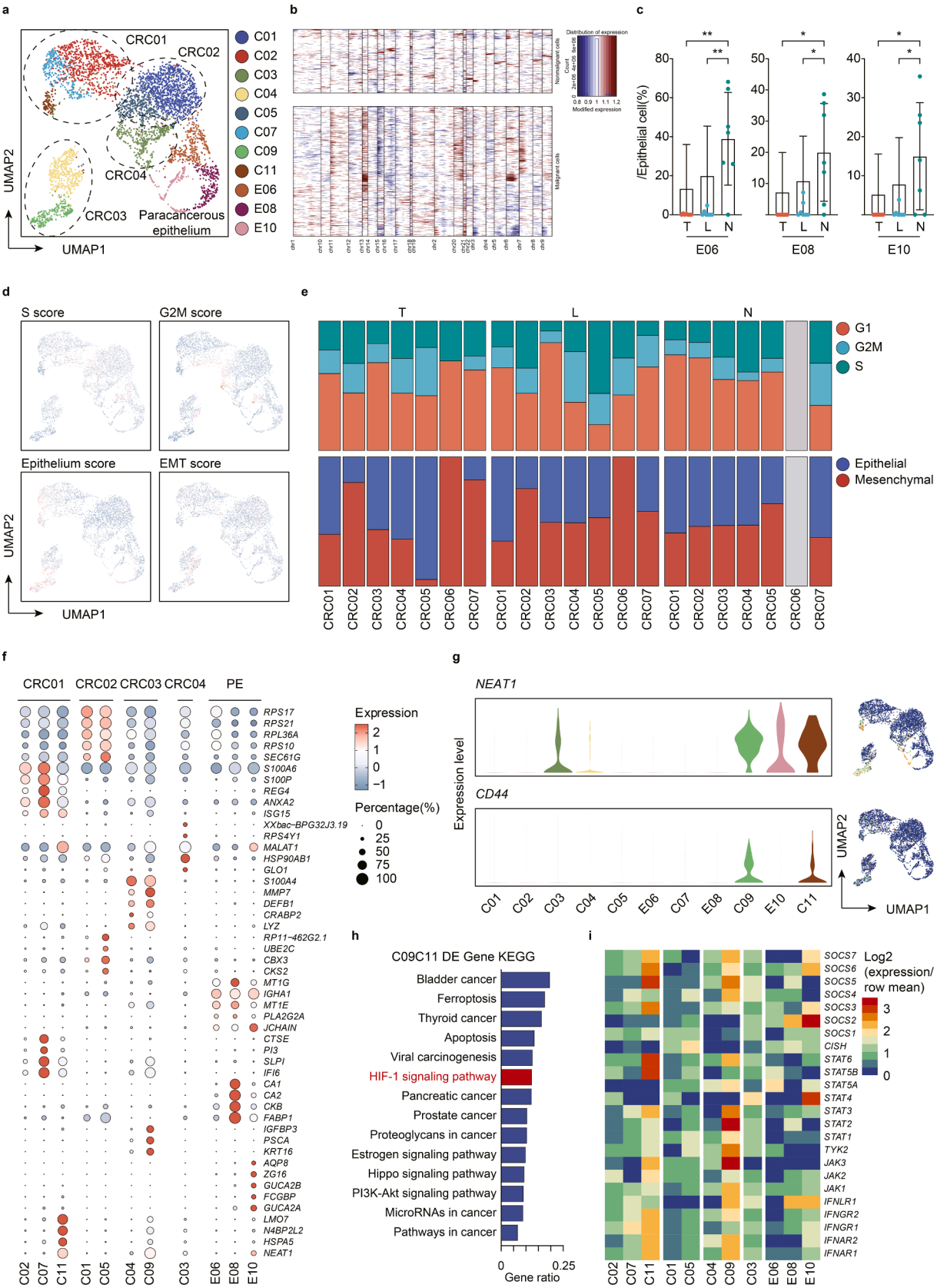

(caption on next page)

Fig. 2. Characteristics of CRC parenchymal cells and activation of JAK-STAT pathway in hypoxic *CD44*+ stem cells.
a. UMAP plot showing 11 clusters of cancer cells (C01, C02, C03, C04, C05, C07, C09, C11) and paracancerous epithelium cells (E06, E08, E10).
b. Copy number variation (CNV) presumption of nonmalignant cells and malignant cells.
c. Scatter plots and statistical differences of nonmalignant cells ($p < 0.05$: * and $p < 0.01$: **).
d. UMAP plot showing S, G2M, differentiation (epithelial or mesenchymal) score (red: high score, blue: low score).
e. Composition of different phases (G1, G2M and S) and states (epithelial or mesenchymal differentiation).
f. Dot plot of top5 genes displaying heterogeneity within and between tumors.
g. Co-expression mode of *NEAT1* and *CD44* showing by violin plots and feature plots.
h. *NEAT1*+*CD44*+ clusters (C09 and C11) KEGG enrichment pathway.
i. Key genes expression heatmap of JAK-STAT pathway.

naïve T cells (T01: *IL7R*+, *CCR7*+), regulatory T cells (Tregs) (T02, T09, T13: *CD4*+, *IL2RA*+, *FOXP3*+, *CTLA4*+), cytotoxic $CD8^+$ T cells (T03: *CD8*+, *GZMA*+, *GZMK*+), MAITs (T04, T05, T06: *KLRD1*-, *TRDC*-, *KLRB1*+), γδT cells (T07: *CD3D*+, *TRDC*+), exhausted CD4 T cells (T08: *CD4*+, *PDCD1*+), NKT cells (T10, T15: *CD3D*+, *KLRD1*+), NK cells (T11: *CD3D*-, *KLRD1*+), memory $CD8^+$ T cells (T12: *CD8*+, *IL7R*+, *CCR7*-) and exhausted $CD8^+$ T cells (T14: *CD8*+, *PDCD1*+, *LAG3*+, *HAVCR2*+). Likewise, re-clustering analysis of B/plasma cells yielded 12 clusters (B01-B12), including plasma cells (B01, B03, B05, B06, B07, B10, B11, B12: *MS4A1*-), memory B cells (B02: *CD38*-, *CD27*+), naïve B cells (B04, B09: *CD38*-, *CD27*-), and plasmablasts (B08: *JCHAIN*+, *MS4A1*+). A total of 13 clusters emerged in myeloid cells (M01-M13), including: macrophages (M01: *CD14*-, *C1QA*+, *C1QB*+), double positive monocytes (M02, M03, M04, M05, M06, M09, M11: CD68+, *CD14*+, *FCGR3A*+), cDCs (M07: *CD1C*+), *CD14*+ monocytes (M08: CD68+, *CD14*+, *FCGR3A*-), neutrophils (M10: *CD68*-, *S100A8*+, *S100A9*+), migDCs (M12: *CCR7*+, *LAMP3*+), and pDCs (M13: *LILRA4*+, *IRF4*+) (Fig. 3**b**).

An in-depth study of the progression to the core region of the tumor showed that the proportion of Treg1 (T02) and naive B2 (B04) increased significantly, whereas the ratio of cDC (M07) substantially diminished (Fig. 3**c**). In previous reports, the stronger regulatory capacity of Tregs with weaker effectiveness of antigen presentation and humoral immune response might be mediated by TGFB signaling, resulting in loss of adaptive immunity within tumors, as evidenced by the inactivation of T cells and their differentiation toward an exhausted phenotype. Accordingly, we probed the expression of functional molecules in the T lymphocytes (Fig. 3**d**). Cytotoxic $CD8^+$ T cells accounted for only a small proportion of total T cells, which expressed intermediate levels of activation molecules, such as *CD27*. The activation of other functional T cell molecules involved in adaptive immunity is less pronounced. Furthermore, MAITs, a component of innate immune cells, were characterized by high expression of *CD40LG*, and T15 in NKT cells also showed upregulated *TIGIT* expression. Although γδT cells have an intermediate expression level of *PRF1*, a sudden drop in expression was minimal in the tumor tissues compared to the L and N sites. Only a fraction of NK cells expressed high levels of cytotoxic-related marker genes such as *GNLY* and *PRF1*. Severe malfunction of the adaptive immune response is deemed one of the pivotal pro-tumoral factors in the immune microenvironment of CRC.

COL11A1+ *tumor-specific CAF remodel microenvironment*

Fibroblasts play an essential role in tumor growth as they serve as an important matrix for oncogenesis. Due to the technical limitations of previous studies, it was difficult to effectively distinguish and analyze parenchymal and mesenchymal cells from tumors. Therefore, the characteristics and functions of some mesenchymal cells have not attracted sufficient attention. At single-cell resolution, we divided CAFs and MFs into 12 heterogeneous clusters (Fig. 4**a**). In light of the distribution characteristics (Fig. 4**b**), cells from F01, F02, and F05 were annotated as MFs in normal tissues, and F04 also had an identical expression pattern to F01 and F02 after taking into account the distributional relationship of the reduction plot. Notably, the cells from F03, F06, and F07 appeared to be predominantly enriched in the T and L regions. And F06 and F07 emerged in T and L regions in each sample of CRC01-CRC07 (**Fig. S1**). Since F07 cells specifically emerged in the T and L regions, it was suggested that cells from F07 represented a type of specialized fibroblast in tumors (Fig. 4**b**). The results of differential gene expression analysis are shown among disparate clusters in Fig. 4**c**, in which F07 had a unique expression profile and specifically expressed *COL11A1,* which can thus be invoked as one of its marker genes. Additionally, this cluster also displayed upregulation of *POSTN, THBS2,* and *TNFRSF12A* (Fig. 4**d**), all of which reportedly facilitates tumorigenesis and the development of CRC. Our study further clarifies the cellular sources of these molecules.

We next systematically investigated the expression levels of several functional molecules in fibroblasts, including marker molecules, matrix metalloproteinases, growth factors, tumor-promoting proteins, and chemokines (Fig. 4**e**). Of note with regard to possible marker genes, F07 highly expressed *FN1* and *SPARC*. High expression of *MMP11, MMP14*, and *TIMP3* may provide favorable conditions for tumor migration. More importantly, F07 widely expressed various growth factors, including *MYDGF, PDGFC, TGFB1*, and *VEGFB*, with upregulated expression of *IGFBP3* and *IGFBP5*, which have been demonstrated to prolong growth stimulation of insulin-like growth factors on tumors. However, they do not appear to play a direct role in chemotaxis. KEGG analysis revealed enrichment of genes associated with TGFB, HIF-1, and stem cells regulating pluripotency signaling pathways in F07 (Fig. 4**f**), indicating its likely important roles in the TME and stem cell remodeling. It has been well established that the WNT signaling pathway is a key player in CRC (Fig. 4**g**). Although we observed no enrichment of genes in the WNT pathway, upregulated *CTNNB1* and *WNT5A* in F07 also likely play a central role, as supported by the protein-protein interaction analysis. Next, we analyzed the evolutionary trajectory among all fibroblasts (Fig. 4**h, i**), in which pseudotime and highly expressed gene heat map clustering identified that F07 was enriched in the middle phase along pseudotime, consistent with roles in promoting tumor growth and shaping the TME.

COL11A1+*INHBA*+ *tumor-specific CAF participates in intercellular communication*

In addition to *COL11A1*, we also found that *INHBA* was significantly expressed in F07 (Fig. 4**d**); therefore, we hypothesized that *COL11A1*+*INHBA*+ tumor-specific CAFs may play an important role in intercellular communication. Considering the lack of spatial information on the RNA profile of the CRC tissue, we carried out spatial transcriptome sequencing from two primary colorectal cancer tissues to verify the existence of *COL11A1*+*INHBA*+ tumor-specific CAFs and to investigate the possibility of intercellular communication between *COL11A1*+*INHBA*+ tumor-specific CAFs and other cell types in primary CRC *in situ* (Fig. 5**a**). We found that the SF03 cluster in the UMAP plot had a phenotype highly similar to that of the F07 cluster (Fig. 5**b, c**). We further verified the existence of this cluster at the protein level by immunohistochemistry (Fig. 5**d**). Next, we studied the expression levels of *ACTA2, COL11A1, INHBA, CD44*, and *HIF1A* in the CRC tissues. The results suggested that *COL11A1*+*INHBA*+ tumor-specific CAFs were concentrated in the core region of tumors with a hypoxic TME, constituting a scaffold for tumor growth (Fig. 5**e**). Although *CD44*+ cells diffused among tumor tissues, the gather of *CD44*+ cells in the hypoxic

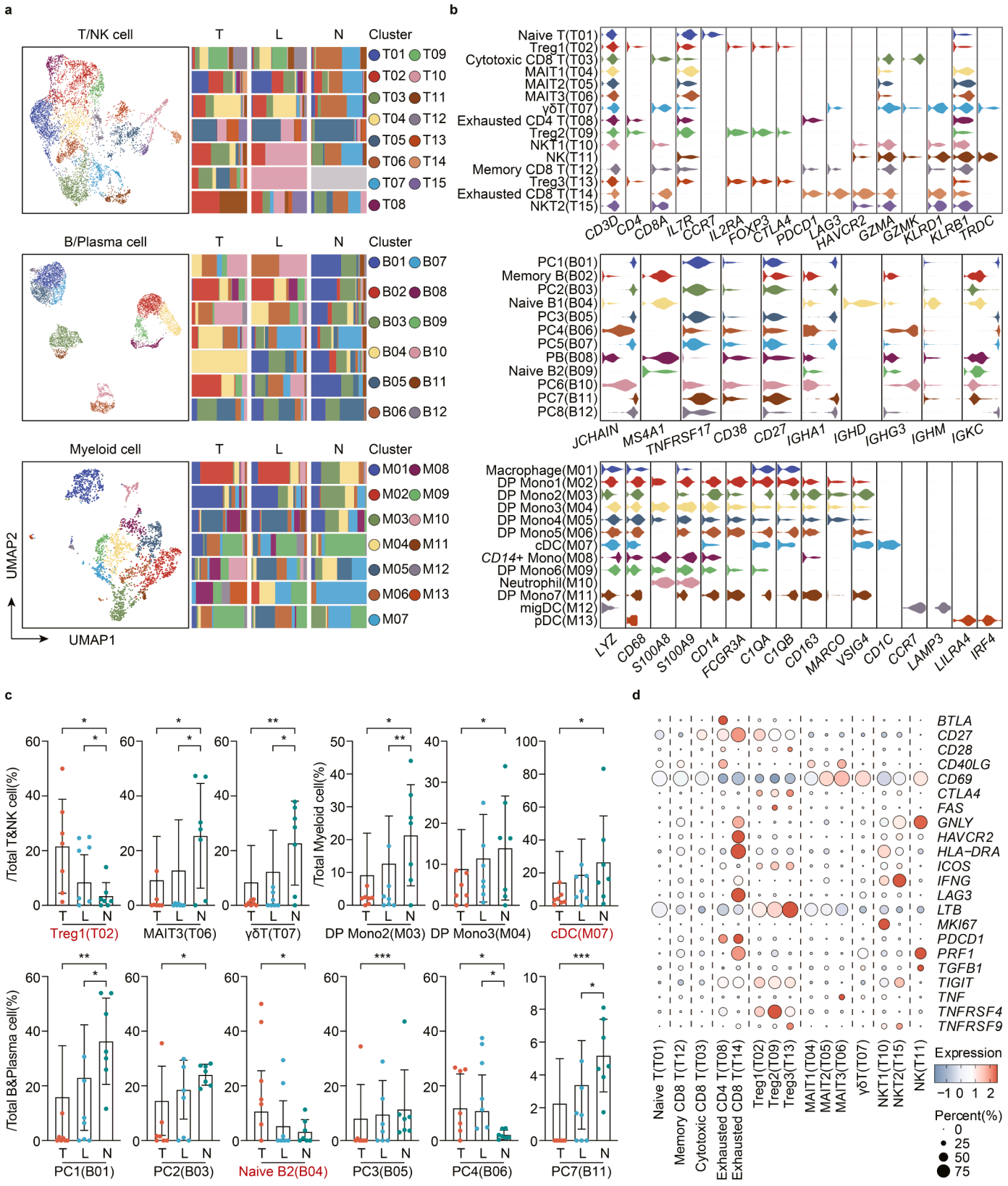

Fig. 3. Antigen presentation decreased in CRC immune microenvironment and Treg negative regulation.
a. UMAP plot of 15 T/NK cell clusters, 12 B/plamsa cell clusters and 13 myeloid cell clusters.
b. Violin plots showing marker genes.
c. Scatter plots of immune cell distribution differences in T, L and N ($p < 0.05$: *, $p < 0.01$: ** and $p < 0.001$ ***).
d. Dot plots of T cell functional genes.

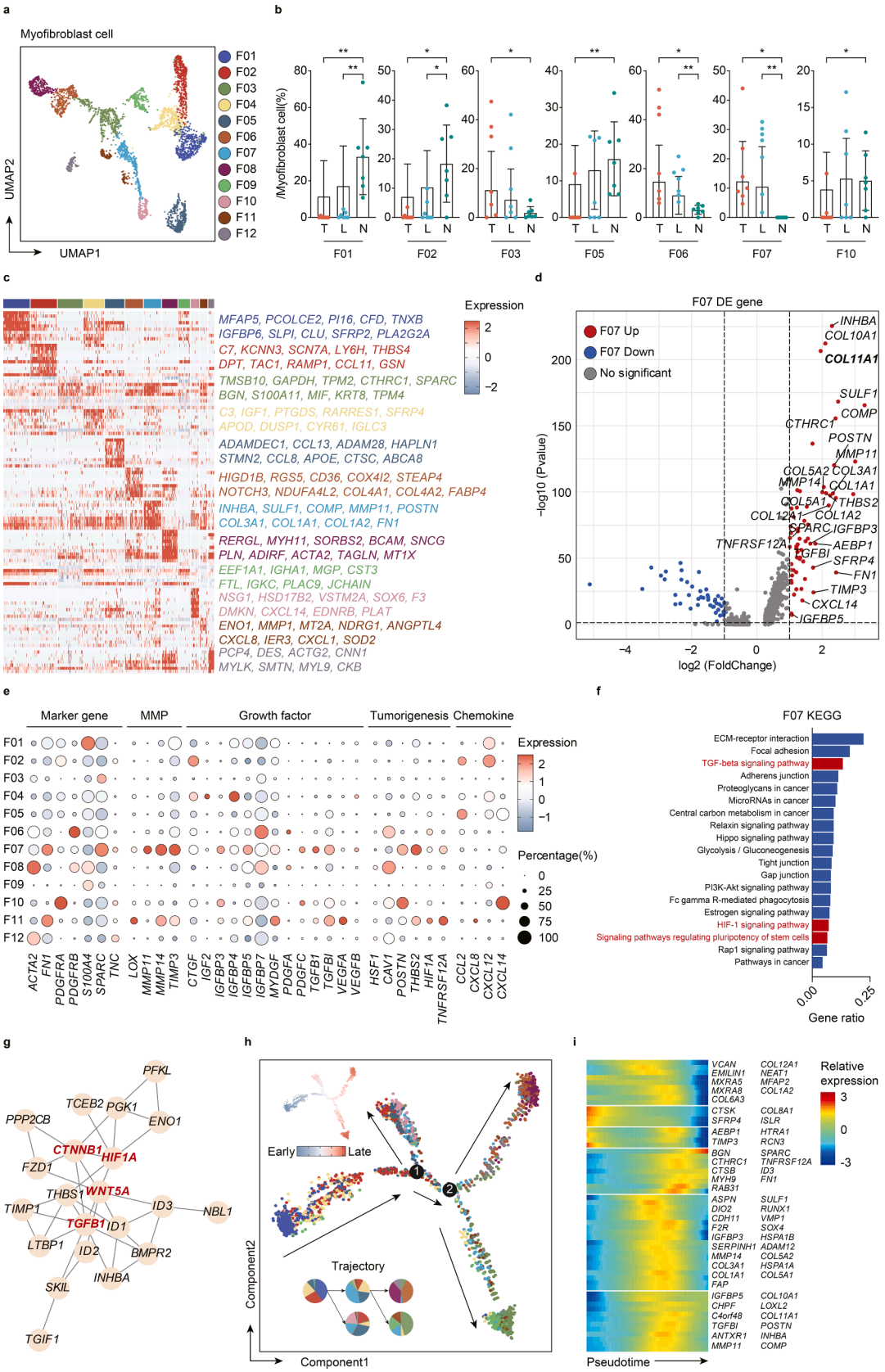

(caption on next page)

Fig. 4. Heterogeneity of cancer-associated fibroblasts (CAFs) and myofibroblasts (MFs) in CRC.
a. UMAP plot of 12 clusters.
b. Distribution and composition of 12 clusters in T (Tumor region), L (Leading-edge region) and N (Non-tumor region) among 7 samples.
c. Scatter plots of distribution differences in T, L and N ($p < 0.05$: * and $p < 0.01$: **).
d. Heatmap displaying differentially expressed (DE) genes.
e. Volcano plot presenting DE genes upregulated in F07 cluster which specifically exists in CRC tumor tissue.
f. Dot plots of marker genes, metal matrix proteins (MMP), growth factors, tumorigenesis proteins and chemokines
g. KEGG pathway enrichment analysis of up-regulating DE genes in F07 cluster.
h. Protein-protein interaction network of TGFB, HIF-1 and stem cells regulating pluripotency pathway.
i. The developmental trajectory of CAFs and MFs, colored-coded by the clusters and pseudo-time.
j. Heatmap displaying expressions of selected upregulating genes in F07 that are arranged along the pseudo-time trajectory.

TME with *COL11A1*+*INHBA*+ tumor-specific CAFs infiltration was observed (Fig. 5**f**).

COL11A1+*INHBA*+ tumor-specific CAFs expressed a variety of significant marker genes that correlated with cell interactions in the CRC microenvironment, including *NRP2, TGFB1, WNT5A, INHBA, MDK, PLXNB2, VEGFB, MRC2*, and *TNFRSF12A* (Fig. 5**g, h**). Based on receptor-ligand interaction analysis, we identified evidence of intensive communication between *NEAT1*+*CD44*+ CSCs (C09 and C11) and key immune cell subgroups (Tregs and cDCs) via these molecules. For example, *VEGFA* can bind to *NRP2* to enhance blood vessel permeability and promote the proliferation and migration of vascular endothelial cells. Tumor necrosis factor receptor superfamily member 12A (TNFRSF12A), also known as fibroblast growth factor-inducible immediate early response protein 14, is a weak inducer of apoptosis in certain cell types and is capable of promoting angiogenesis and endothelial cell proliferation. Although it is activated in the early stage of tumorigenesis, *TGFB1* mainly exerts anti-cancer effects; with the downregulation of receptors on tumor cells, highly expressed *TGFB1* can exert immunosuppressive functions, which inhibit activation and differentiation of T/B lymphocytes, resulting in immune dysregulation and immune escape. Based on the cell–cell communication analysis, cells from C09 and C11 were found to have completely divergent reactivity with respect to the *TGFB1-TGFBR3* axis. In addition, the secretion of *TGFB1* can regulate Tregs and cDCs via *TGFBR1* and *TGFBR2*, respectively.

Notably, the secretion of INHBA by tumor-specific *COL11A1*+*INHBA*+ CAFs could directly act on stem phenotype cells through ACVR receptors, which heightens the risk of a high tumor burden through the activin pathway. Multiple immunohistochemical analyses showed that *COL11A1*+*INHBA*+ CAFs were spatially close to $ACVR^{+}CD44^{+}$ cancer cells in CRC tissue, offering opportunities for direct intercellular communication (Fig. 5**i**).

We used the TCGA database to validate the association between *COL11A1* and *INHBA* with the prognosis of patients who developed malignant tumors, and found that patients with high expression of *COL11A1* and *INHBA* had a markedly worse clinical prognosis (Fig. 5**j**).

Altogether, these results suggest that *COL11A1*+*INHBA*+ tumor-specific CAFs may play a crucial role in maintaining cancer cell stemness and promoting tumor progression, thereby leading to adverse outcomes.

High expression of INHBA protein in CRC tumors predicts poor survival

To further evaluate the prognostic value of INHBA among patients with CRC, we performed immunohistochemistry on our CRC tissue microarrays. INHBA protein expression was quantified based on artificial intelligence learning (Fig. 6**a**). The H-Score of 179 CRC patients ranged from 0.4136 to 66.1938, and we divided these into low-expression ($n = 60$), moderate-expression ($n = 60$), and high-expression groups ($n = 59$) based on the H-Score (Fig. 6**b**). We analyzed the baseline data of 179 patients with CRC and found that age, sex, tumor location, preoperative CEA, preoperative CA199, pTNM stage, differentiation, and adjuvant therapy were not significantly different among the three groups (Table 1). Kaplan–Meier analysis showed that patients with high INHBA protein expression levels had shorter disease-free survival than those with moderate or low INHBA protein expression (all $p < 0.05$) (Fig. 6**c**).

Discussion

With the rapid development of sequencing technology, scRNA-seq has become an important tool for analyzing tumor heterogeneity. scRNA-seq analysis enables comparisons between normal and tumor tissue, and has led to the emergence of a comprehensive interpretation of the distribution and subtype characteristics of cells across disparate regions. In this study, our results showed heterogeneous characteristics of parenchymal cells, immune cells, and CAFs in CRC.

Among the single-cell landscapes of different regions in CRC, we discovered a novel heterogeneous cluster of tumor-specific CAFs overexpressing COL11A1. CAFs are key players in the TME and are known to secrete various factors that contribute to the maintenance of colorectal cancer stem cells (CSCs), chemoresistance, and metastasis [6,11,12]. Although many studies have described the heterogeneity of CAFs in CRC, there is still a lack of markers that accurately reflect their different phenotypes and functions [7]. Our results suggest that *COL11A1* is a marker for a cluster of tumor-specific cancer-promoting CAFs in CRC. Collagen is the major extracellular matrix molecule that provides support for cell growth and is responsible for the mechanical resilience of connective tissues [13]. Abnormally expressed collagen can enhance malignancy and the ability of tumor cells to escape the immune system by combining and storing bioactive molecules such as cytokines and growth factors that regulate the TME [14], and which are associated with the prognosis of various cancer types, including CRC [15]. *COL11A1* is the gene encoding COL11A1, a fibrillary collagen which is mainly distributed in cartilaginous tissues [16]. Its deficiency is associated with skeletal and chondroid disorders [17,18]. Although high expression of *COL11A1* has been reported to indicate poor prognosis in CRC [19] and the gene is overexpressed in CAFs compared to normal fibroblasts [6], few studies have focused on the mechanisms of *COL11A1*+ tumor-specific activation of CAFs and its possible functions in CRC.

In our study, we found that a cluster of CAFs specifically emerged in tumor regions, suggesting the existence of tumor-specific CAFs in CRC. Differential gene expression analysis showed that the cluster of CAFs had a unique expression profile and specifically expressed *COL11A1*. Hence, *COL11A1*+ tumor-specific CAFs were used in our study. *COL11A1*+ tumor-specific CAFs upregulated a series of genes with known roles in facilitating tumorigenesis, providing favorable conditions for tumor migration, or prolonging growth stimulation of insulin-like growth factors. This suggests that these CAFs may have pivotal roles in promoting CRC development. Among the upregulated genes, *INHBA* was specifically overexpressed in the *COL11A1*+ tumor-specific CAFs. *INHBA* encodes inhibin subunit beta A (INHBA), which belongs to the transforming growth factor (TGF) superfamily [20]. INHBA homodimers are known bioactive proteins that exist in various tissues [21–24], and are implicated in multiple biological processes, including neoplastic progression [25,26]. *INHBA* is predominantly expressed in stage IV CRC [27]. However, few studies have focused on the mechanisms underlying INHBA secretion by *COL11A1*+ tumor-specific CAFs and the regulation

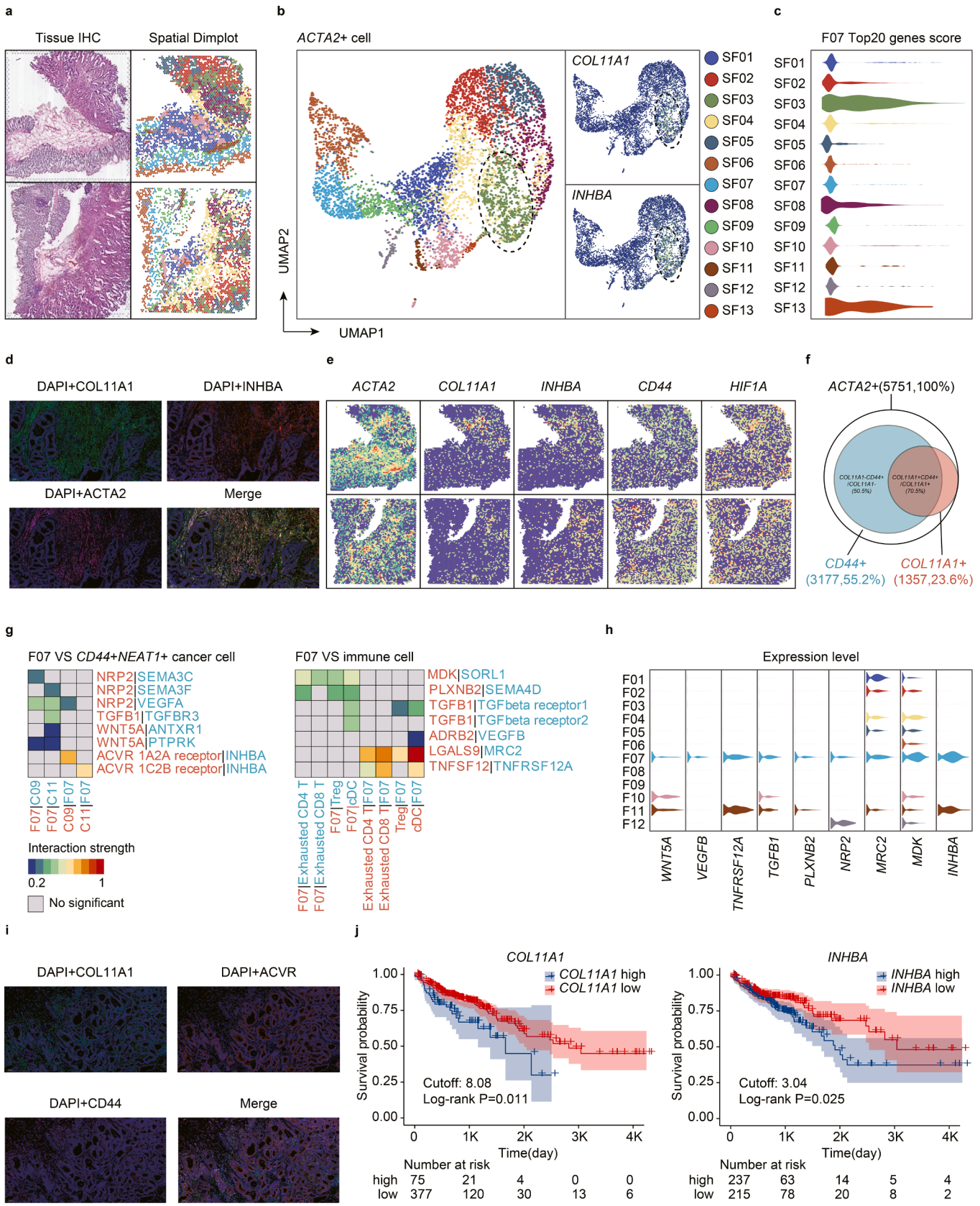

(caption on next page)

Fig. 5. The distribution of *COL11A1*+*INHBA*+ F07 *in situ* and its Intercellular Communication.
a. Spatial transcriptome single-cell sequencing clusters distribution overlayed with tissue immunohistochemistry (IHC).
b. UMAP plots showing the co-localization of *COLA11A1* and *INHBA*.
Violin plots displaying F07 top 20 genes score of SF01-13.
c. Multiple immunohistochemistry verified co-localization of COL11A1, INHBA, and ACTA2 at protein level.
d. The expression of *ACTA2, COL11A1, INHBA, CD44*, and *HIF1A* in spatial level.
e. The Venn diagram showing the overlap of spots with *ACTA2, CD44*, and *COL11A1* expression in two CRC tissue samples with spatial transcriptomics data analysis
f. Cell-to-cell communication heatmap among F07, *CD44*+*NEAT1*+ cancer cells and immune cells.
g. Violin plots displaying communication molecules expression in CAFs and MFs.
h. Multiple immunohistochemistry verified co-localization of COL11A1, ACVR, and CD44 at protein level.
i. The Kaplan–Meier (KM) curves presenting the prognosis disparity of *COL11A1* and *INHBA* expression in TCGA database.

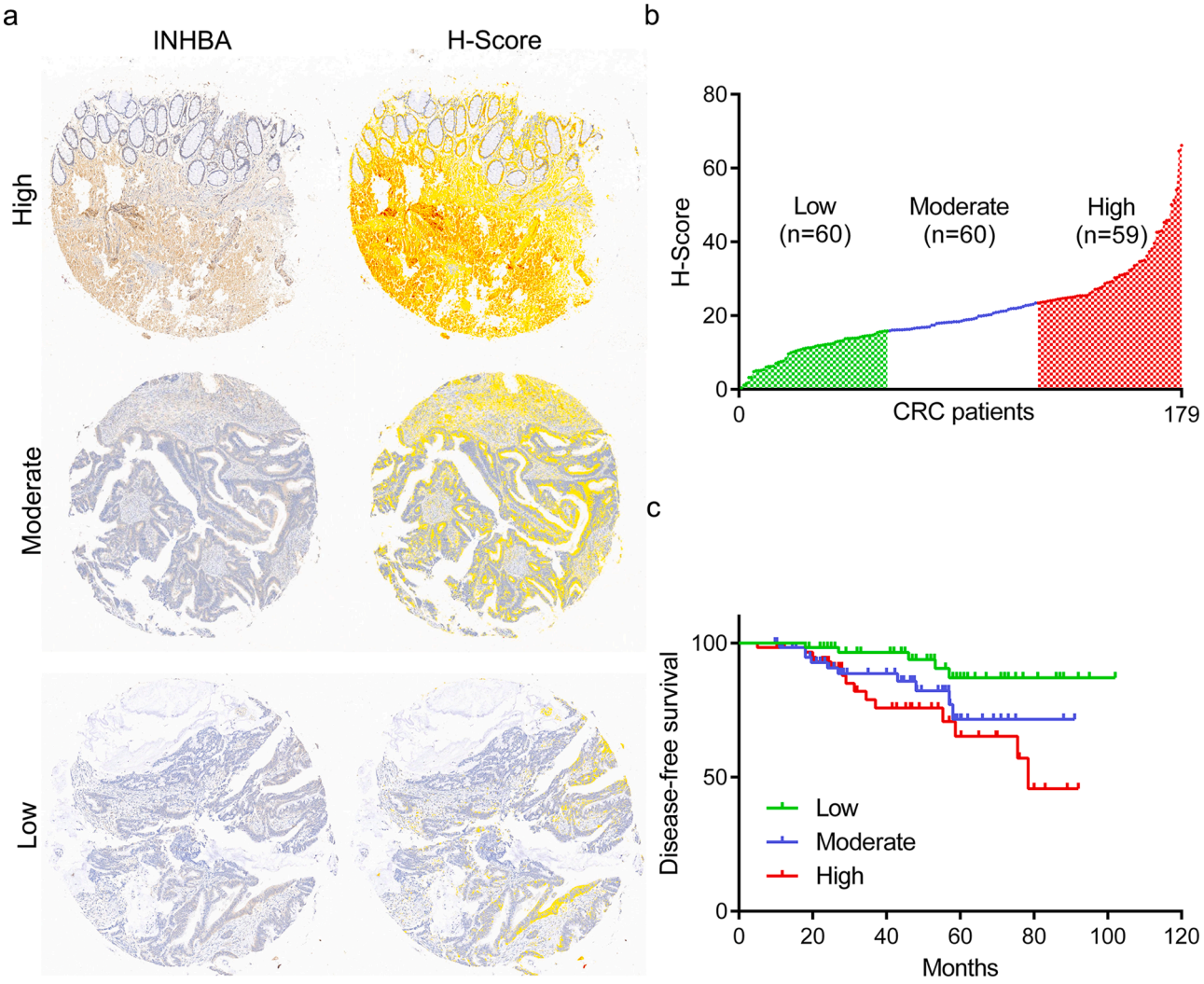

Fig. 6. Association between INHBA expression and patient survival in CRC.
a. Representative images for INHBA immunostaining in CRC tissues.
b. H-SCORE of immunohistochemistry distribution and group division in 179 CRC patients.
c. The Kaplan–Meier (KM) curves presenting the prognosis disparity of INHBA expression in 179 CRC patients.

of CRC cells.

Our results revealed that 1) *COL11A1*+ tumor-specific CAFs were enriched in the middle phase along pseudotime; 2) TGFB, HIF-1, and stem cells regulating pluripotency signaling pathways were activated, and 3) *HIF1A* played a central role in the protein-protein interaction network. Hence, we inferred that upon activation under a hypoxic TME, *COL11A1*+ tumor-specific CAFs increase INHBA secretion through TGFB signaling pathways, which promote tumor growth, shape the TME, and remodel cancer cell stemness. Hypoxia, a critical feature of the TME, promotes cancer stemness during tumor growth [28]. Hypoxia inducible factor-1α (HIF-1α), a vital transcription factor for cell sensing and adaptation to hypoxia, plays an important role in normal metabolism [29]. For example, HIF-1α helps chondrocytes adapt to the hypoxic environment in cartilaginous tissues under normal physiological conditions [30]. Considering that COL11A1 is expressed mainly in cartilaginous tissue [16], we can extrapolate that HIF-1α may have a potential effect in regulating COL11A1 secretion. Previous studies have revealed that HIF-1α is upregulated in CRC patients and is associated with poor prognosis [31,32], suggesting a role of HIF-1α in CRC tumorigenesis, although how hypoxic TME regulates CAFs for

Table 1
Comparison of clinicopathological characteristics among patients with low, moderate, and high INHBA expression.

clinicopathological characteristics		INHBA expression Low	Moderate	High	*p* value
Age (year)		61.80 ±11.366	60.30 ±13.177	61.47 ±12.675	0.786
Gender (n, %)	Male	36 (60.0)	33 (55.0)	39 (66.1)	0.464
	Female	24 (40.0)	27 (45.0)	20 (33.9)	
Tumor location (n, %)	Rectum	39 (65.0)	31 (51.7)	34 (57.6)	0.333
	Colon	21 (35.0)	29 (48.3)	25 (42.4)	
preoperative CEA (n, %)	<5ng/ml	36 (60.0)	33 (55.0)	43 (72.9)	0.116
	≥5ng/ml	24 (40.0)	27 (45.0)	16 (27.1)	
preoperative CA199 (n, %)	<37U/ml	52 (86.7)	54 (90.0)	51 (86.4)	0.802
	≥37U/ml	8 (13.3)	6 (10.0)	8 (13.6)	
pTNM stage (n, %)	I	5 (8.3)	7 (11.7)	8 (13.6)	0.132
	II	28 (46.7)	38 (63.3)	26 (44.1)	
	III	27 (45.0)	15 (25.0)	25 (42.4)	
Differntiation (n, %)	High	7 (11.7)	5 (8.3)	2 (3.39)	0.41
	Moderate	50 (83.3)	54 (90.0)	55 (93.2)	
	Poor	3 (5.0)	1 (1.7)	2 (3.29)	
Adjuvant Therapy (n, %)	Yes	9 (15.0)	12 (20.0)	15 (25.4)	0.366
	No	51 (85.0)	48 (80.0)	44 (74.6)	

maintenance of cancer cell stemness and chemoresistance is unclear. In this study, verifying the existence of *COL11A1*+ tumor-specific CAFs might partly answer these questions.

Our spatial transcriptome sequencing and data from multiple immunofluorescent staining experiments successfully verified the existence of *COL11A1*+*INHBA*+ tumor-specific CAFs in primary CRC *in situ*. These CAFs are located in the core region of tumors, potentially constituting a scaffold for tumor growth. The data further showed that *COL11A1*+*INHBA*+ tumor-specific CAFs were enriched in hypoxic regions in which *HIF1A* is upregulated and with neighboring CD44+ CRC cells. Analysis of potential receptor-ligand interactions suggested that *COL11A1* tumor-specific CAFs communicate between $CD44^+$ CRC cells in the hypoxic TME and key immune cell subgroups (Tregs and cDCs) via a series of molecules overexpressed in the *COL11A1* tumor-specific CAFs. Among these molecules, INHBA strongly interacts with ACVR in $CD44^+$ CRC cells. Previous studies have revealed that the INHBA homodimer-ACVR-SMAD2/3 signaling network in pancreatic cancer plays a pivotal role in regulating multiple mechanisms key to the development of chemoresistance, including enhancement of stem cell-like properties and tumorigenicity of pancreatic cancer cells, mediating cooperative interactions between pancreatic cancer cells and the surrounding stroma, and regulating the deposition of extracellular matrix proteins within the TME [20]. Here, we infer that under a hypoxic TME, *COL11A1*+ tumor-specific CAFs maintain the stemness of CRC cells through a ligand-receptor interaction between INHBA and ACVR.

Despite advances in the diagnostic and therapeutic tools for CRC, there is still a desperate need for better risk stratification tools. Here, we not only reconfirmed that CRC patients with high expression of *COL11A1* or *INHBA* had a markedly worsening clinical prognosis using the TCGA dataset, but also explored the expression of INHBA in a well-characterized cohort of CRC and scored the protein expression using a digital pathological image analysis software. With the help of artificial intelligence learning tools, quantification of the expression of the INHBA protein by immunohistochemistry becomes feasible and reliable, which makes it a usable tool for prognostic analysis in CRC patients.

However, this study has some limitations. First, there is insufficient proof that cluster F07 identified in the single-cell sequencing data and cluster SF03 found in the spatial transcriptome sequencing data had the exact same phenotype. Second, bulk RNA analysis from the TCGA database cannot detect the cell types that contribute to RNA expression levels. Third, we were not able to cleanly isolate CAFs and quantify the expression of INHBA in tissue microarrays. Finally, some clinicopathological parameters such as vascular invasion, perineural invasion, and microsatellite instability were not included in this analysis.

In conclusion, we propose that the hypoxic TME specifically activates *COL11A1*+ tumor-specific CAFs through HIF-1α. *COL11A1*+ tumor-specific CAFs act as cancer-promoting CAFs by secreting a series of molecules that interact with CRC cells and key immune cell subgroups. *COL11A1*+ tumor-specific CAFs markedly overexpress INHBA via the TGFB signaling pathway. INHBA promotes CRC development by binding to ACVR in CRC cells and is a potential marker for predicting CRC prognosis.

Materials and methods

scRNA-seq datasets availability

Raw single-cell RNA data were deposited in the ArrayExpress database of EMBL-EBI (www.ebi.ac.uk/arrayexpress) with accession number E-MTAB-8107. Detailed clinicopathological information of the seven CRC patients is available in the Supplementary Materials of the article published in Cell Research (2020) 0:1–18 (https://doi.org/10.1038/s41422-020-0355-0).

Single-cell RNA-seq data analysis

Analyses were performed by using R software version 4.0.3 and the 'Seurat' package version 3.1.1, 'Monocle2' package version 2.18.0, 'infercnv' package version 1.6.0, 'corrplot' package version 0.92, and CellphoneDB Python 3.8.5. Cells with less than 200 detectable genes and mitochondrial content greater than 10% were filtered out during the quality control process. After excluding low-quality cells, we then used the 'NormalizeData' function to normalize filtered UMI counts, for which the normalization method is set as 'logNormalize', with a scaling factor of 10000. The 'FindVariableGenes' function was conducted with default parameters in order to select highly variable genes, which were subsequently applied for linear dimensionality reduction. Next, principal component analysis (PCA) was performed using the top 2000 highly variable genes via the 'RunPCA' function. Afterwards, a number of PCs were selected corresponding to ElbowPlot, followed by performing the 'RunUMAP' function with a perplexity value of 30 to acquire bidimensional coordinates for single cells. Meanwhile, we used unsupervised cell clustering by 'FindClusters' function with a resolution of 0.6 based on identical PCs as for 'RunUMAP' function. The datasets were visualized using UMAP plots. Based on normalized data, function "FinAllMarkers" or "FindMarkers" were used to identify DEGs across different clusters. We applied the Bonferroni correction method to adjust the *P* value and excluded DEGs whose adjusted P value was higher than 0.05. The non-parametric Wilcoxon rank sum test from the "Seurat" package was designated for differential expression analysis between each subpopulation.

Spatial transcriptomics data analysis

CRC tissues were collected from a CRC patient who underwent radical resection at the Department of Colorectal Surgery, Changhai Hospital, Naval Medical University, Shanghai, China. Two tissue samples from the primary tumor were collected. The CRC tissues were pretreated, snap-frozen with dry ice, cut into 10 μm thick cryosections, and mounted onto spatial transcriptomics arrays. Each spot had a diameter of 100 μm and spots were 200 μm from center to center, covering an area of 6.1 × 6.5 mm^2. The spots were printed with approximately 2×10^8 oligonucleotides containing an 18-mer spatial barcode, randomized 7-mer (unique molecular identifier) UMI, and

poly- 20TVN transcript capture region.

After tissue permeabilization, cDNA synthesis, and probe release, the barcoded mRNA/cDNA material was cleaved from the arrays and sequencing libraries were prepared in solution. Second-strand cDNA was synthesized, followed by *in vitro* transcription and adapter ligation. Sequencing handles and indexes were added to the PCR mix, and the completed libraries were sequenced on the 10x Genomics platform (Illumina NextSeq, HiSeq4000, or NovaSeq6000) with paired-end sequencing.

Cell cycle and differentiation analysis and pseudo-time transcriptional trajectory analysis

Based on the expression of genes related to G2/M and S phases as well as differentiation (epithelial and mesenchymal) states, cells are categorized into particular cell cycle and differentiation stages. Briefly, we applied the "CellCycleScoring" function to calculate the cell cycle and differentiation scores for each cell, followed by matching to the metadata.

The "Monocle2" package was used for trajectory and pseudo-time analysis containing 400 marker genes from the "differentialGeneTest" function, which is designed to infer potential pedigree differentiation trajectories. RNA counts in all cells from clusters were selected as input to "Monocle2" for downstream analyses. A generalized additive model (GAM) was constructed to generate an average expression for each isotype. The lineage difference trajectory among CAFs and MFs clusters was performed using default parameters of "Monocle" after dimensionality reduction and cell ordering.

Cell-cell interacting network analysis

To gain insight into potential interactions between disparate cell types, we performed cell-cell network analysis to investigate potential ligand-receptor pairs using "CellPhoneDB". Predicted receptor-ligand interactions across different cell types were confirmed, corresponding to the expression level of receptors in one cell type and the expression level of homogenous ligands in another cell type. Bonferroni multiple test correction was used to adjust the *P* value; a ligand-receptor pair with an adjusted *P* value less than 0.01 was deemed a potential molecular partner in mediating cell-to-cell communication.

Multiple immunofluorescence staining

Co-staining of CRC tissues was performed using antibodies against COL11A1 (21841-1-AP, Proteintech, 1:100) and INHBA (10651-1-AP, Proteintech, 1:100).

ACVR1(10227-T24, SinoBiological, 1:100), ACTA2 (19245, CST, 1:100), and CD44 (ab189524, Abcam, 1:100) were detected using a Four-color Fluorescence kit (Recordbio Biological Technology, Shanghai, China) based on the tyramide signal amplification (TSA) technology according to the manufacture's instruction. Briefly, paraffin sections of CRC tissues were treated with antigen retrieval buffers under optimal conditions, and then blocked successively with 3% H_2O_2 and 3% BSA-PBS. After incubation with the primary antibody overnight at 4°C and horseradish peroxidase (HRP) secondary antibody for 50 min at room temperature, 100 μl of TYR-520 (1:500), TYR-570 (1:300), TYR-690 (1:500), and DAPI were used successively for staining.

Tissue microarray immunohistochemical assay

Clinicopathological parameters were collected from 179 patients with CRC who underwent surgical resection at Changhai Hospital, Naval Medical University (Shanghai, China), between January 2001 and November 2011. Informed consent was obtained. Tissue microarrays were constructed from the donated CRC tissue specimens using a commercial company (Outdo Biotech, Shanghai, China). One core was used for each sample, with a core diameter of 1.2 mm. The TNM stage was reclassified according to the American Joint Committee on Cancer staging manual (seventh edition). This study was approved by the Institutional Review Board of Changhai Hospital.

INHBA staining on tissue microarrays was performed using an IHC kit (Servicebio Technology, Wuhan, China) according to the manufacturer's instructions. Specimens were stained with antibodies. The sections were heated at 70°C for 1 h, dewaxed in xylene, and dehydrated through a gradient concentration of alcohol. After retrieving and blocking endogenous peroxidase and nonspecific staining with 3% H_2O_2 and normal bovine serum, the sections were incubated with primary antibody overnight at 4°C. The slides were then incubated with HRP-conjugated secondary antibody for 10 min at 37°C. Finally, the sections were visualized by diaminobenzidine (DAB) solution and counterstained with haematoxylin. The stained tissue microarray slides were analyzed at a resolution of × 20 (digital scanning via K-Viewer software; KFBIO Co., Ningbo, Zhejiang, China). INHBA protein expression was quantified using Aipathwell software (Servicebio Technology, Wuhan, China), a digital pathological image analysis software based on artificial intelligence learning. The H-SCORE of each core was evaluated using the following formula: H-SCORE=$\sum$ (pi × i) = (percentage of weak intensity × 1) + (percentage of moderate intensity × 2)+(percentage of strong intensity × 3).

Statistical analysis

All statistical analyses were performed using the R software (version 4.0.3) and GraphPad Prism software version 8.0. All grouped data were summarized as mean ± standard error of the mean (SEM). Unpaired Student's *t*-test and one-way analysis of variance (ANOVA) were used to determine the statistical significance of the comparison between two groups and more than three groups, respectively. Two-tailed *P* values less than 0.05 were considered to be statistically significant. Survival analysis was conducted using the Kaplan–Meier method.

Credit authorship contribution statement

W.Z. and F.C designed the study and drafted the manuscript. N.Z., R. W., L.Z., and Z.L. prepared the tables and figures and drafted the manuscript. Q.M. and K.Z. contributed to the clinical sample collection. All authors participated in revising the manuscript. All authors contributed to the article and approved the submitted version.

Figure S1. Distribution and composition of 12 clusters of cancer-associated fibroblasts (CAFs) and myofibroblasts (MFs) in T (Tumor region), L (Leading-edge region) and N (Non-tumor region) among 7 samples.

Declaration of Competing Interest

The authors declare that they have no known competing financial interests or personal relationships that could have appeared to influence the work reported in this paper.

Acknowledgments

The results here are in whole or part based upon data generated by the TCGA Research Network: https://www.cancer.gov/tcga. The authors thank the TCGA Research Network.

The authors thank the National Natural Science Foundation of China (82072750) and Natural Science Fund of Shanghai (20ZR1457200) for the funding of this study. The experimental protocol was approved by Shanghai Changhai Hospital Ethics Committee (CHEC2017-235, Shanghai, China).

Supplementary materials

Supplementary material associated with this article can be found, in the online version, at doi:10.1016/j.tranon.2022.101570.

References

[1] E Dekker, PJ Tanis, JLA Vleugels, PM Kasi, MB. Wallace, Colorectal cancer, Lancet 394 (10207) (2019) 1467–1480.
[2] GK Dy, TJ Hobday, G Nelson, HE Windschitl, MJ O'Connell, SR Alberts, et al., Long-term survivors of metastatic colorectal cancer treated with systemic chemotherapy alone: a North Central Cancer Treatment Group review of 3811 patients, N0144, Clin. Colorectal Cancer 8 (2) (2009) 88–93.
[3] H Kobayashi, A Enomoto, SL Woods, AD Burt, M Takahashi, DL. Worthley, Cancer-associated fibroblasts in gastrointestinal cancer, Nat. Rev. Gastroenterol. Hepatol. 16 (5) (2019) 282–295.
[4] R Nussinov, CJ Tsai, H. Jang, Anticancer drug resistance: An update and perspective, Drug Resist. Updat. 59 (2021), 100796.
[5] MJ Bissell, WC. Hines, Why don't we get more cancer? A proposed role of the microenvironment in restraining cancer progression, Nat. Med. 17 (3) (2011) 320–329.
[6] YA Tang, YF Chen, Y Bao, S Mahara, S Yatim, G Oguz, et al., Hypoxic tumor microenvironment activates GLI2 via HIF-1alpha and TGF-beta2 to promote chemoresistance in colorectal cancer, Proc. Natl. Acad. Sci. U. S. A. 115 (26) (2018) E5990–E5999.
[7] V Koliaraki, CK Pallangyo, FR Greten, G. Kollias, Mesenchymal cells in colon cancer, Gastroenterology 152 (5) (2017) 964–979.
[8] E Sahai, I Astsaturov, E Cukierman, DG DeNardo, M Egeblad, RM Evans, et al., A framework for advancing our understanding of cancer-associated fibroblasts, Nat. Rev. Cancer 20 (3) (2020) 174–186.
[9] H Kobayashi, KA Gieniec, JA Wright, T Wang, N Asai, Y Mizutani, et al., The balance of stromal BMP signaling mediated by GREM1 and ISLR drives colorectal carcinogenesis, Gastroenterology 160 (4) (2021) 1224–39e30.
[10] S Wang, Q Zhang, Q Wang, Q Shen, X Chen, Z Li, et al., NEAT1 paraspeckle promotes human hepatocellular carcinoma progression by strengthening IL-6/STAT3 signaling, Oncoimmunology 7 (11) (2018), e1503913.
[11] D Hanahan, LM. Coussens, Accessories to the crime: functions of cells recruited to the tumor microenvironment, Cancer Cell 21 (3) (2012) 309–322.
[12] S Su, J Chen, H Yao, J Liu, S Yu, L Lao, et al., CD10(+)GPR77(+) cancer-associated fibroblasts promote cancer formation and chemoresistance by sustaining cancer stemness, Cell 172 (4) (2018) 841-56 e16.
[13] A Sorushanova, LM Delgado, Z Wu, N Shologu, A Kshirsagar, R Raghunath, et al., The collagen suprafamily: from biosynthesis to advanced biomaterial development, Adv. Mater. 31 (1) (2019), e1801651.
[14] HS Abyaneh, M Regenold, TD McKee, C Allen, MA. Gauthier, Towards extracellular matrix normalization for improved treatment of solid tumors, Theranostics 10 (4) (2020) 1960–1980.
[15] EM Carter, CL. Raggio, Genetic and orthopedic aspects of collagen disorders, Curr. Opin. Pediatr. 21 (1) (2009) 46–54.
[16] M Bernard, H Yoshioka, E Rodriguez, M Van der Rest, T Kimura, Y Ninomiya, et al., Cloning and sequencing of pro-alpha 1 (XI) collagen cDNA demonstrates that type XI belongs to the fibrillar class of collagens and reveals that the expression of the gene is not restricted to cartilagenous tissue, J. Biol. Chem. 263 (32) (1988) 17159–17166.
[17] SW Tompson, CA Bacino, NP Safina, MB Bober, VK Proud, T Funari, et al., Fibrochondrogenesis results from mutations in the COL11A1 type XI collagen gene, Am. J. Hum. Genet. 87 (5) (2010) 708–712.
[18] O Khalifa, F Imtiaz, R Allam, Z Al-Hassnan, A Al-Hemidan, K Al-Mane, et al., A recessive form of Marshall syndrome is caused by a mutation in the COL11A1 gene, J. Med. Genet. 49 (4) (2012) 246–248.
[19] H Fischer, R Stenling, C Rubio, A. Lindblom, Colorectal carcinogenesis is associated with stromal expression of COL11A1 and COL5A2, Carcinogenesis 22 (6) (2001) 875–878.
[20] M Abdel Mouti, S Pauklin, TGFB1/INHBA Homodimer/Nodal-SMAD2/3 signaling network: a pivotal molecular target in PDAC treatment, Mol. Ther. 29 (3) (2021) 920–936.
[21] K Ogawa, M Funaba, Y Chen, M. Tsujimoto, Activin A functions as a Th2 cytokine in the promotion of the alternative activation of macrophages, J. Immunol. 177 (10) (2006) 6787–6794.
[22] LH Katz, Y Li, JS Chen, NM Munoz, A Majumdar, J Chen, et al., Targeting TGF-beta signaling in cancer, Expert Opin. Ther. Targets 17 (7) (2013) 743–760.
[23] E Meulmeester, P Ten Dijke, The dynamic roles of TGF-beta in cancer, J. Pathol. 223 (2) (2011) 205–218.
[24] YY Sheen, MJ Kim, SA Park, SY Park, JS. Nam, Targeting the transforming growth factor-beta signaling in cancer therapy, Biomol. Ther. 21 (5) (2013) 323–331.
[25] K Yoshinaga, K Yamashita, K Mimori, F Tanaka, H Inoue, M. Mori, Activin a causes cancer cell aggressiveness in esophageal squamous cell carcinoma cells, Ann. Surg. Oncol. 15 (1) (2008) 96–103.
[26] K Yoshinaga, K Mimori, K Yamashita, T Utsunomiya, H Inoue, M. Mori, Clinical significance of the expression of activin A in esophageal carcinoma, Int. J. Oncol. 22 (1) (2003) 75–80.
[27] S Wildi, J Kleeff, H Maruyama, CA Maurer, MW Buchler, M. Korc, Overexpression of activin A in stage IV colorectal cancer, Gut 49 (3) (2001) 409–417.
[28] B Keith, RS Johnson, MC. Simon, HIF1alpha and HIF2alpha: sibling rivalry in hypoxic tumour growth and progression, Nat. Rev. Cancer 12 (1) (2011) 9–22.
[29] V Plaks, N Kong, Z. Werb, The cancer stem cell niche: how essential is the niche in regulating stemness of tumor cells? Cell Stem Cell 16 (3) (2015) 225–238.
[30] S Stegen, K Laperre, G Eelen, G Rinaldi, P Fraisl, S Torrekens, et al., HIF-1alpha metabolically controls collagen synthesis and modification in chondrocytes, Nature 565 (7740) (2019) 511–515.
[31] D Cao, M Hou, YS Guan, M Jiang, Y Yang, HF. Gou, Expression of HIF-1alpha and VEGF in colorectal cancer: association with clinical outcomes and prognostic implications, BMC Cancer 9 (2009) 432.
[32] S Rasheed, AL Harris, PP Tekkis, H Turley, A Silver, PJ McDonald, et al., Hypoxia-inducible factor-1alpha and -2alpha are expressed in most rectal cancers but only hypoxia-inducible factor-1alpha is associated with prognosis, Br. J. Cancer 100 (10) (2009) 1666–1673.